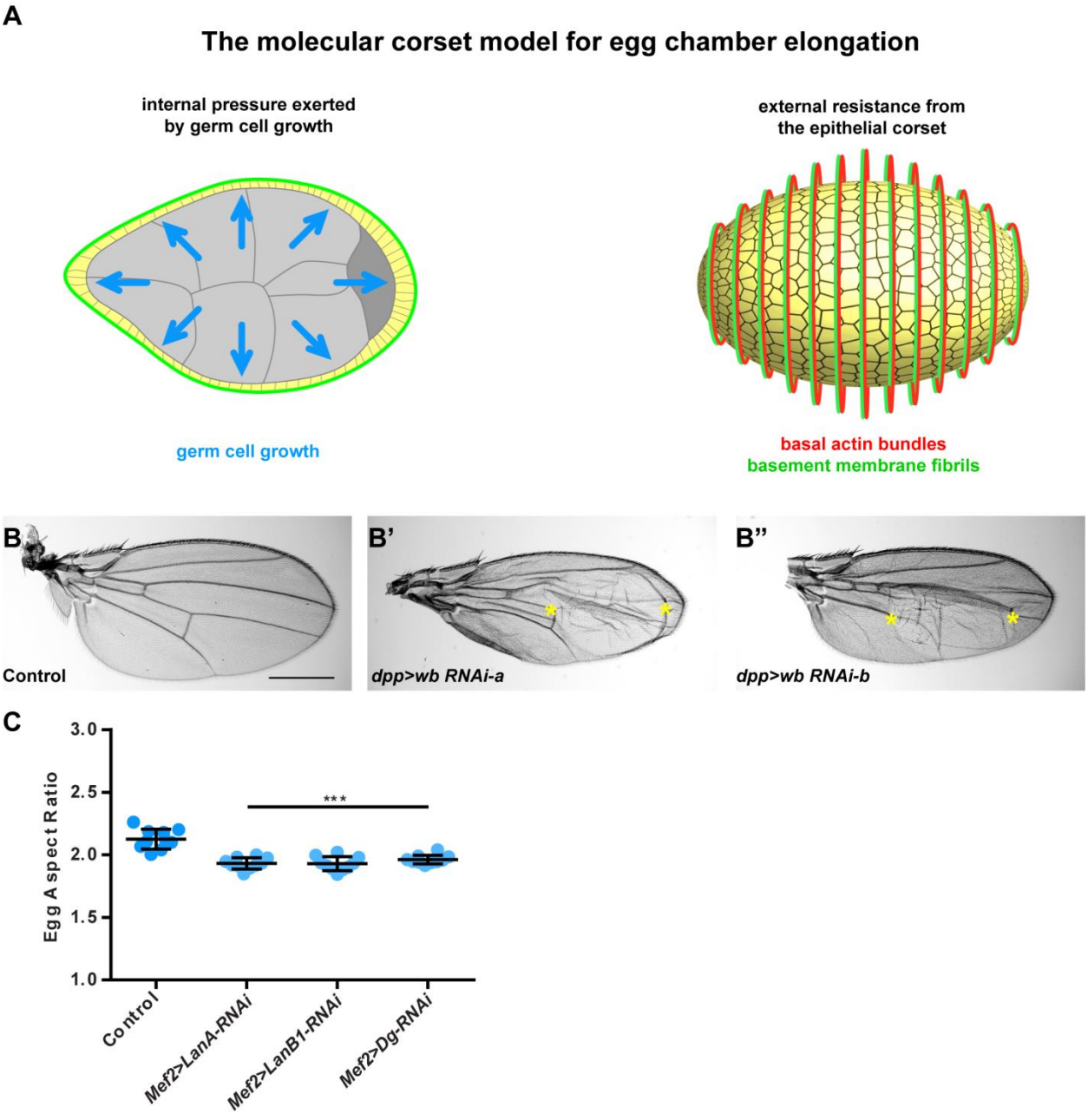

Figure S1. *wb-RNAi* validation and depletion of LanA, LanB1 & Dg with *Mef2-Gal4*

(A) Overview of the molecular corset model for egg chamber elongation. (B) Both *wb-RNAi* transgenes used in this study produce blisters in adult wings (yellow stars) when driven with *decapentaplegic-Gal4* (*dpp-Gal4*). Scale bar = 500 µm. (C) Using *Mef2-Gal4* to deplete LanA, LanB1 or Dg from the muscle sheath reduces the egg's aspect ratio. Data represent mean ± s.d., *t*-test *** = P<0.001. n = 9-10 eggs per condition.

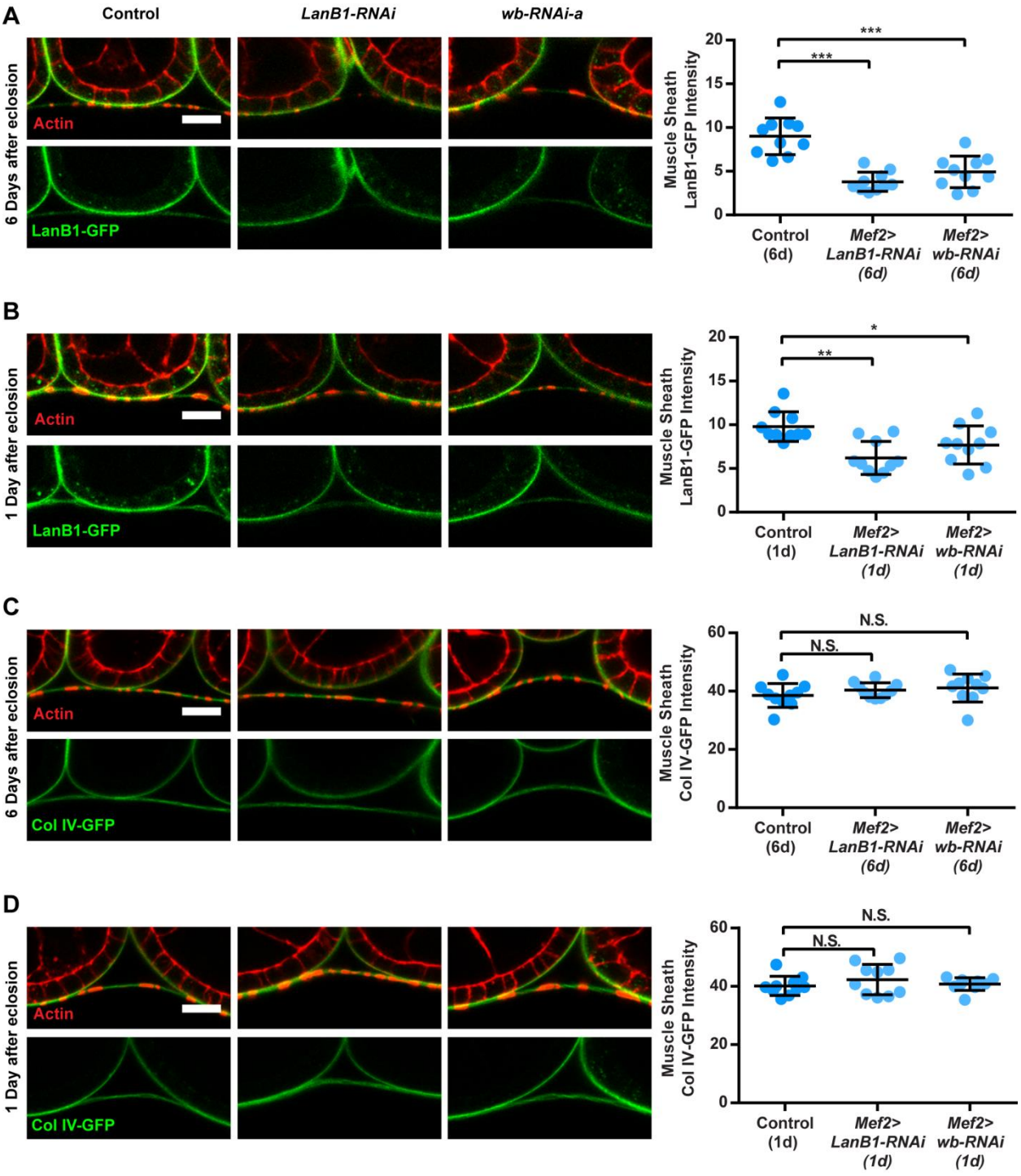

Figure S2. *Mef2>LanB1-RNAi and Mef2>wb-RNAi-a* both reduce Laminin levels in muscle sheath BMs, without disrupting Col IV levels

(A-B) *Mef2>LanB1-RNAi and Mef2>wb-RNAi-a* both reduce Laminin levels in muscle sheath BMs. Laminin levels are monitored using 1 copy of a *LanB1-GFP* fosmid transgene, where LanB1 is expressed under its endogenous promoter. Both RNAi transgenes reduce LanB1-GFP levels compared to controls; however, the effect is stronger for *LanB1-RNAi* than for *wb-RNAi*. This difference is expected, as LamininA and LamininW both appear to be expressed in the muscle sheath, and LanB1 is a subunit of both isoforms, whereas Wb is only a subunit of one. The reduction in LanB1-GFP is also higher for both RNAi transgenes 6 days after eclosion (A) compared to 1 day after eclosion (B). (C-D) In contrast, the same set of RNAi conditions has no effect on the levels of the other major BM protein, Collagen IV. Collagen IV levels are monitored using one copy of a GFP protein trap in the Collagen IV α2 chain Viking. (A-D) Data represent mean ± s.d., *t*-test * = P<0.05, ** = P<0.01, *** = P<0.001. n = 10 ovarioles per condition.

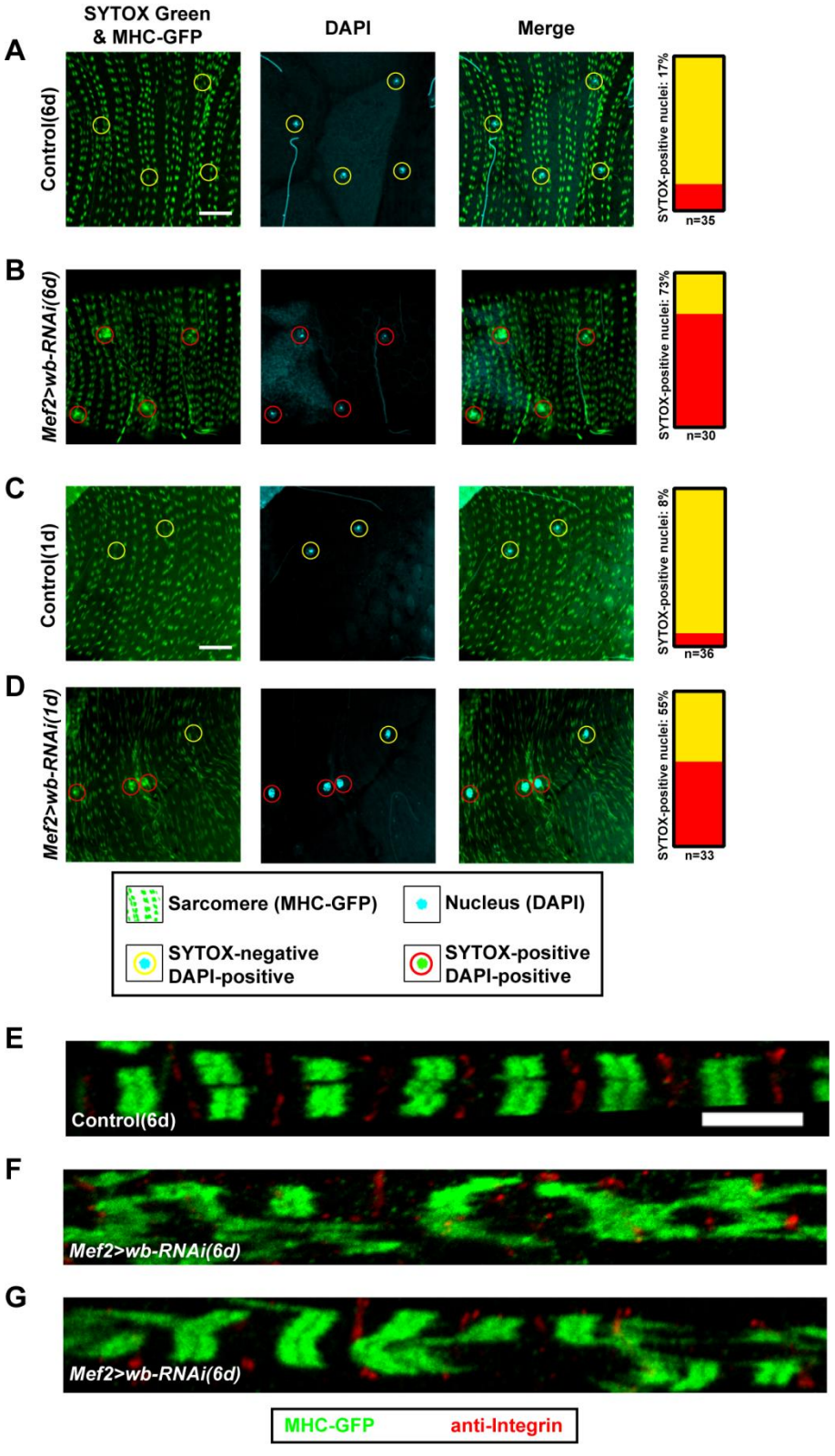

Figure S3. Wb depletion causes damage to the muscle sheath

(A-D) SYTOX Green labelling of muscle sheath nuclei identifies cells whose plasma membranes have been breached. Representative images showing the muscle sheath sarcomeres labelled with Myosin Heavy Chain GFP (MHC-GFP) and muscle sheath nuclei labelled with DAPI. Nuclei that are co-labelled with SYTOX Green are circled in red and those that lack SYTOX green are circled in yellow. Scale bars = 20 µm. Graphs show the percentage of labelled nuclei for each condition. Increased labelling is seen under both *Mef2>wb-RNAi(6d)* (A-B) and *Mef2>wb-RNAi(1d)* (C-D). (E-G) Micrographs showing the sarcomeric structure of the muscle sheath. MHC-GFP marks the A-band (green) and anti-integrin-βPS marks the Z-discs (red). (E) Image showing normal sarcomere structure in a control muscle sheath. Scale bar = 5 µm. (F,G) Under *Mef2>wb-RNAi(6d)* the muscle fibers begin to tear and sarcomeres become highly disorganized.

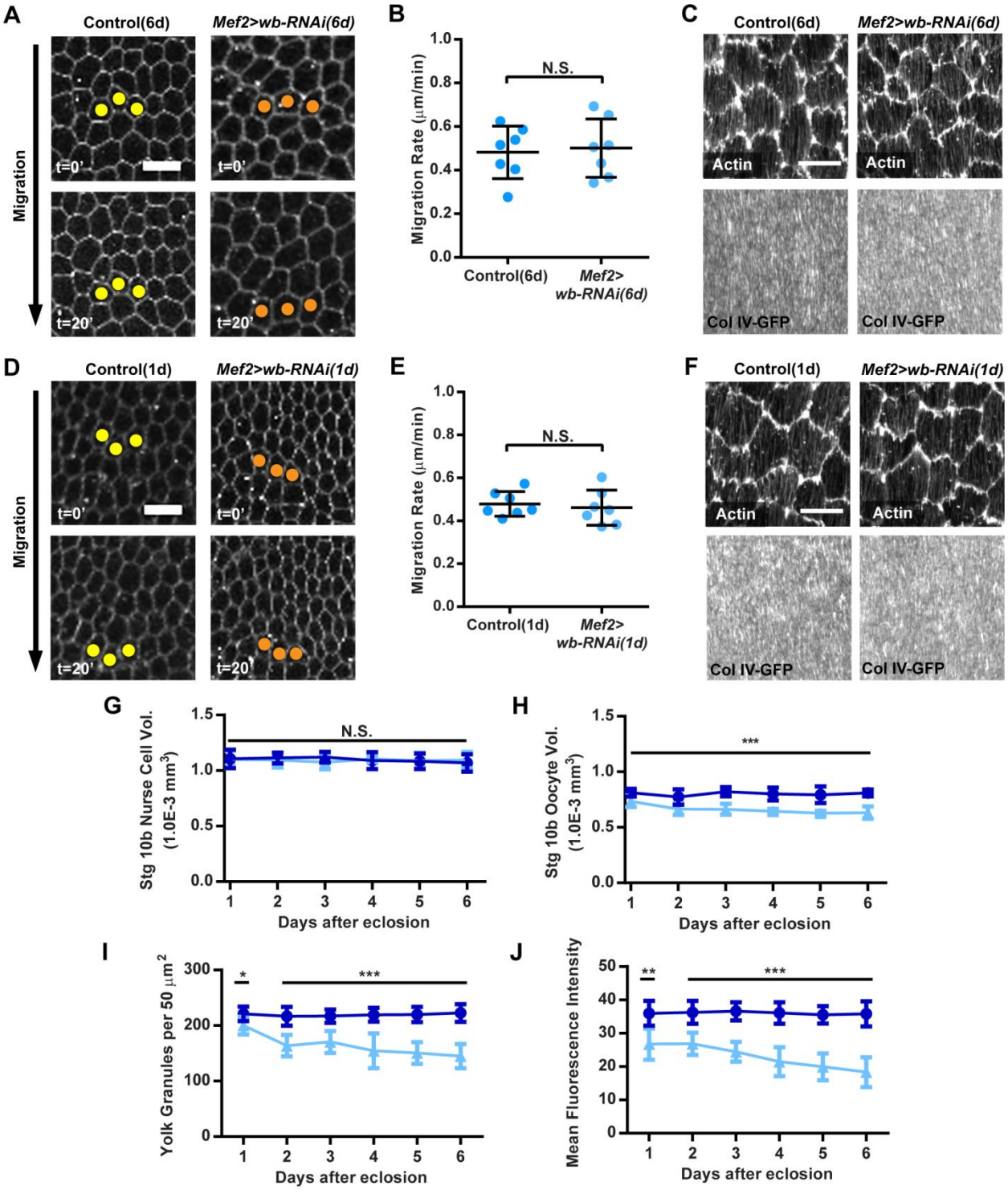

Figure S4. Effect of *Mef2>wb-RNAi* on the molecular corset & vitellogenesis time course

(A-F) The molecular corset in the follicular epithelium is normal in stage 7 egg chambers under both the *Mef2>wb-RNAi(6d)* and *Mef2>wb-RNAi(1d)* conditions. (A,D) Stills from representative movies showing that the follicle cells migrate normally under *Mef2>wb-RNAi*. Colored dots mark the same three cells between the two time points for each condition. (B,E) Graphs quantifying the effects shown in (A,D). (C,F) Representative images of the basal actin bundles and polarized basement membrane showing that their organization is unaffected by *Mef2>wb-RNAi.* The actin bundles are marked with rhodamine-phalloidin and the basement membrane with a GFP protein trap in the Collagen IV α2 chain Viking. (A,C,D,F) Scale bars = 10 μm. (G-J) A time-course experiment shows that Wb depletion from the muscle sheath causes an increasing defect in vitellogenesis over time. Wb was depleted from the muscle sheath and four phenotypes were measured in stage 10b egg chambers each day for six days: (G) nurse cell volume, (H) oocyte volume, (I) yolk granule density and (J) yolk granule auto-fluorescence. (G-J) All values except nurse cell volume decrease over time. Data represent mean ± s.d., *t*-test * = P<0.05, ** = P<0.01, *** = P<0.001. n = 10 egg chambers per condition per day.

Movie 1. *Mef2>wb-RNAi(6d)* largely eliminates ovarian contractions

Movie showing the contractile activity of a single cultured ovary from either a Control(6d) (left) or *Mef2>wb-RNAi(6d)* (right) female. Length = 1 min.

Movie 2. *Mef2>wb-RNAi(6d)* does not affect egg chamber rotation

Movie showing that rotation occurs normally in stage 7 egg chambers from both Control(6d) (left) and *Mef2>wb-RNAi(6d)* (right) females. Cell membranes are marked with CellMask. Laser-scanning confocal images. Length = 20 min/ 1 min intervals. Scale bar = 20 μm.

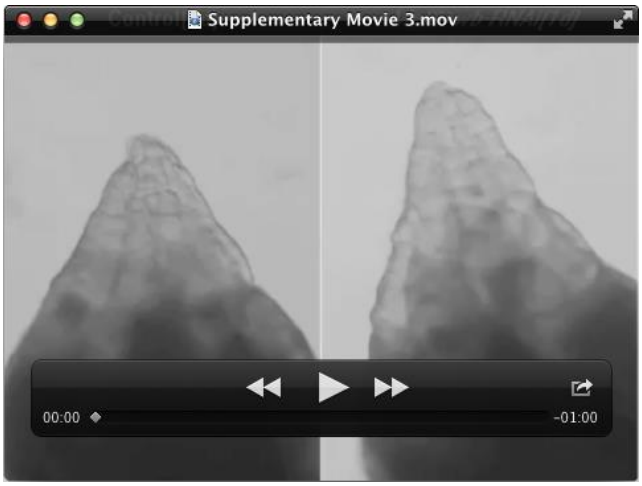

Movie 3. *Mef2>wb-RNAi(1d)* increases the frequency of ovarian contractions

Movie showing the contractile activity of a single cultured ovary from either a Control(1d) (left) or *Mef2>wb-RNAi(1d)* (right) female. Length = 1 min.

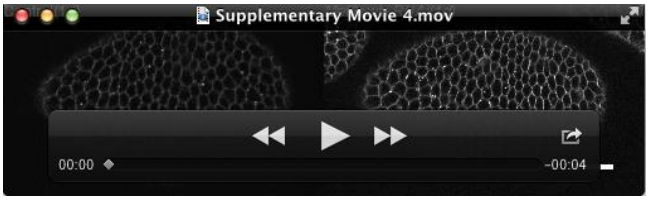

Movie 4. *Mef2>wb-RNAi(1d)* does not affect egg chamber rotation

Movie showing that rotation occurs normally in stage 7 egg chambers from both Control(1d) (left) and *Mef2>wb-RNAi(1d)* (right) females. Cell membranes are marked with CellMask. Laser-scanning confocal images. Length = 20 min/ 1 min intervals. Scale bar = 20 μm.

SUPPLEMENTARY MATERIALS AND METHODS

Measurements of BM protein levels in the muscle sheath

Ovaries were fixed and stained with phalloidin, and images were taken of central transverse sections through isolated ovarioles. In ImageJ, lines with a width of 10 pixels were then drawn over regions of the muscle sheath that were not in contact with an egg chamber, and the mean fluorescence intensity of either Col IV-GFP or LanB1-GFP was measured along those lines. At least four measurements of this type were made for each ovariole. These values were then averaged and displayed as a single data point. Confocal settings were held constant for all experiments with a given GFP transgene.

Measurement of egg chamber rotation rates

Ovaries were dissected in live imaging media as described (Prasad et al., 2007). CellMask dye (1:1000, Thermofisher) was added to the live imaging media to mark cell membranes. Ovarioles were transferred in live imaging media + CellMask to an agar pad (live imaging media with 0.4% NuSieve GTG low-melt agarose) that was formed on a gas permeable membrane slide (Sarstedt Inc, catalog # 94.6150.101). Most of the live imaging media was removed from the pad and a coverslip was placed on top of the sample, stabilized with vacuum grease at each corner. The coverslip was then gently compressed onto the sample and halocarbon oil 27 (Sigma) was added around the coverslip to keep the media from evaporating. Egg chambers were imaged with a 40/1.3 numerical aperture (NA) EC Plan-NeoFluor oil-immersion objective on a laser-scanning confocal microscope (Zeiss LSM510) controlled by the LSM acquisition software. ImageJ was used for image processing. To determine rotation rates, kymographs were generated from movies of rotating egg chambers, and the migration rate was measured as the slope of lines corresponding to cell membranes moving over time.

SYTOX Green staining

Freshly dissected ovaries were incubated in S2 media with SYTOX Green (1:5000, Invitrogen) and DAPI (1:1000, Sigma) for 15 minutes, washed with PBS, and fixed for 15 minutes in PBS + formaldehyde. Ovarioles were separated with forceps and mounted in antifade. Images were taken of muscle sheath overlaying stage 10 egg chambers for quantification of labelled nuclei, with confocal settings held constant among all conditions.

Hemolymph collection and processing

A hemolymph collection chamber was fabricated using a 20 gauge needle to make four holes in the base of a 0.5 mL microcentrifuge tube, and then placing that tube inside a 1.5 mL microcentrifuge tube. A 33 gauge needle was then used to puncture the dorsal thorax of four adult females, which were loaded into the smaller tube and centrifuged at 4°C for 5 minutes at 5600 rpm. The smaller tube was discarded and 2 µL of hemolymph buffer (S2 media + protease inhibitor cocktail (1:100, Sigma p2714) was added to the hemolymph in the larger tube. To dilute this sample, 1 µL was added to a new tube containing 8 µL of hemolymph buffer. 1.33 µL of this dilution was then added to a new tube containing 8 µL of hemolymph buffer and 8 µL of SDS-Page sample buffer.

Table S1 References for RNAi transgenes

RNAi transgene	Reference
UAS-wb-RNAi$^{TRiP.JF03238}$	(Papagiannouli et al., 2014)
UAS-wb-RNAi^{v108020}	(Kim and Choe, 2014) (Han et al., 2012)
UAS-LanA-RNAi$^{TRiP.JF02908}$	(Papagiannouli et al., 2014) (Kim and Choe, 2014)
UAS-LanB1-RNAi^{v23121}	(Kim and Choe, 2014)
UAS-Dg-RNAi^{v107029}	(Kim and Choe, 2014)

Table S2 Detailed experimental genotypes and conditions

Fig.	Panel	Genotype	Temp for cross	Females on yeast	
				Temp	No. days
2	B	*tj-Gal4/ +; UAS-mCD8-GFP/ +*	25°C	25°C	2
	C	*tj-Gal4/ +*	RT	29°C	6
		tj-Gal4/ +; UAS-wb-RNAi$^{TRiP.JF03238}$	RT	29°C	6
		tj-Gal4/ UAS-wb-RNAi^{v108020}	RT	29°C	6
	D	*Mef2-Gal4/ UAS-mCD8-GFP*	25°C	25°C	2
	E	*Mef2-Gal4/ +*	RT	29°C	6
		Mef2-Gal4/ UAS-wb-RNAi$^{TRiP.JF03238}$	RT	29°C	6
		TubP-Gal80^{ts}/ +; Mef2-Gal4/ +	18°C	29°C	6
		TubP-Gal80^{ts}/ UAS-wb-RNAi^{v108020}; Mef2-Gal4/ +	18°C	29°C	6
	F	*tj-Gal4, Mef2-Gal80/ +; UAS-mCD8-GFP/ +*	25°C	25°C	2
	G	*tj-Gal4, Mef2-Gal80/ +*	RT	29°C	6
		tj-Gal4, Mef2-Gal80/ +; UAS-LanA-RNAi$^{TRiP.JF02908}$	RT	29°C	6
		tj-Gal4, Mef2-Gal80/ +; UAS-wb-RNAi$^{TRiP.JF03238}$	RT	29°C	6
3	B C	*MHC-GFP/ +; Mef2-Gal4/ +*	RT	29°C	5
		MHC-GFP/ +; Mef2-Gal4/ UAS-wb-RNAi$^{TRiP.JF03238}$	RT	29°C	5
	D	*Mef2-Gal4/ +*	RT	29°C	6
	E F	*Mef2-Gal4/ +*	RT	29°C	6
		Mef2-Gal4/ UAS-wb-RNAi$^{TRiP.JF03238}$	RT	29°C	6
4	A-F	*Mef2-Gal4/ +*	RT	29°C	6
		Mef2-Gal4/ UAS-wb-RNAi$^{TRiP.JF03238}$	RT	29°C	6
5	A-C	*Mef2-Gal4/ +*	RT	29°C	6
		Mef2-Gal4/ UAS-wb-RNAi$^{TRiP.JF03238}$	RT	29°C	6
	D-G	*w^{1118}*	RT	29°C	1
		Yp1^{ts}/ Df(1)C52	RT	29°C	1
6	B-E	*vkg-GFP*	25°C	25°C	3
		Host: Ovo^{D1} v^{24}/ + Donor: vkg-GFP	25°C	25°C	3
7	A-C	*w^{1118}*	RT	25°C	1
		sn^{G409E}	RT	25°C	1
		bwk^{151}/bwk^{08482}	RT	25°C	1
8	A	*Mef2-Gal4/ +*	RT	29°C	1-7
		Mef2-Gal4/ UAS-wb-RNAi$^{TRiP.JF03238}$	RT	29°C	1-7
	B	*Mef2-Gal4/ +*	RT	29°C	1-7
		UAS-Dg-RNAi^{v107029}/ +; Mef2-Gal4/ +	RT	29°C	1-7
	C D	*MHC-GFP/ +; Mef2-Gal4/ +*	RT	29°C	1
		MHC-GFP/ +; Mef2-Gal4/ UAS-wb-RNAi$^{TRiP.JF03238}$	RT	29°C	1
	E	*Mef2-Gal4/ +*	RT	29°C	1

	F G	*Mef2-Gal4/ +*	RT	29°C	1
		Mef2-Gal4/ UAS-wb-RNAi$^{TRiP.JF03238}$	RT	29°C	1
9	A-E H J	*Mef2-Gal4/ +*	RT	29°C	1
		Mef2-Gal4/ UAS-wb-RNAi$^{TRiP.JF03238}$	RT	29°C	1
	G I	*Mef2-Gal4/ +*	RT	29°C	6
		Mef2-Gal4/ UAS-wb-RNAi$^{TRiP.JF03238}$	RT	29°C	6
S1	B	*dpp-Gal4/ +*	25°C	25°C	3
		dpp-Gal4/ UAS-wb-RNAi$^{TRiP.JF03238}$	25°C	25°C	3
		UAS-wb-RNAi^{v108020}/ +; dpp-Gal4/+	25°C	25°C	3
	C	*Mef2-Gal4/ +*	RT	29°C	6
		Mef2-Gal4/ UAS-LanA-RNAi$^{TRiP.JF02908}$	RT	29°C	6
		Mef2-Gal4/ UAS-LanB1-RNAi^{v23121}	RT	29°C	6
		UAS-Dg-RNAi^{v107029}/ +; Mef2-Gal4/ +	RT	29°C	6
S2	A	*Mef2-Gal4, LanB1-GFP/ +*	RT	29°C	6
		Mef2-Gal4, LanB1-GFP/UAS-LanB1-RNAi^{v23121}	RT	29°C	6
		Mef2-Gal4, LanB1-GFP/ UAS-wb-RNAi$^{TRiP.JF03238}$	RT	29°C	6
	B	*Mef2-Gal4, LanB1-GFP/ +*	RT	29°C	1
		Mef2-Gal4, LanB1-GFP/UAS-LanB1-RNAi^{v23121}	RT	29°C	1
		Mef2-Gal4, LanB1-GFP/ UAS-wb-RNAi$^{TRiP.JF03238}$	RT	29°C	1
	C	*vkg-GFP/ +; Mef2-Gal4/ +*	RT	29°C	6
		vkg-GFP/ +; Mef2-Gal4/ UAS-LanB1-RNAi^{v23121}	RT	29°C	6
		vkg-GFP/ +; Mef2-Gal4/ UAS-wb-RNAi$^{TRiP.JF03238}$	RT	29°C	6
	D	*vkg-GFP/ +; Mef2-Gal4/ +*	RT	29°C	1
		vkg-GFP/ +; Mef2-Gal4/ UAS-LanB1-RNAi^{v23121}	RT	29°C	1
		vkg-GFP/ +; Mef2-Gal4/ UAS-wb-RNAi$^{TRiP.JF03238}$	RT	29°C	1
S3	A E	*MHC-GFP/+; Mef2-Gal4/ +*	RT	29°C	6
	B F G	*MHC-GFP/+; Mef2-Gal4/ UAS-wb-RNAi$^{TRiP.JF03238}$*	RT	29°C	6
	C	*MHC-GFP/+; Mef2-Gal4/ +*	RT	29°C	1
	D	*MHC-GFP/+; Mef2-Gal4/ UAS-wb-RNAi$^{TRiP.JF03238}$*	RT	29°C	1
S4	A B	*Mef2-Gal4/ +*	RT	29°C	6
		Mef2-Gal4/ UAS-wb-RNAi$^{TRiP.JF03238}$	RT	29°C	6
	C	*vkg-GFP/ +; Mef2-Gal4/ +*	RT	29°C	6
		vkg-GFP/ +; Mef2-Gal4/ UAS-wb-RNAi$^{TRiP.JF03238}$	RT	29°C	6
	D E	*Mef2-Gal4/ +*	RT	29°C	1
		Mef2-Gal4/ UAS-wb-RNAi$^{TRiP.JF03238}$	RT	29°C	1
	F	*vkg-GFP/ +; Mef2-Gal4/ +*	RT	29°C	1
		vkg-GFP/ +; Mef2-Gal4/ UAS-wb-RNAi$^{TRiP.JF03238}$	RT	29°C	1
	G-J	*Mef2-Gal4/ +*	RT	29°C	1-6
		Mef2-Gal4/ UAS-wb-RNAi$^{TRiP.JF03238}$	RT	29°C	1-6

SUPPLEMENTARY REFERENCES

Han, C., Wang, D., Soba, P., Zhu, S., Lin, X., Jan, L. Y. and Jan, Y. N. (2012). Integrins regulate repulsion-mediated dendritic patterning of drosophila sensory neurons by restricting dendrites in a 2D space. *Neuron* **73**, 64-78.

Kim, M. J. and Choe, K. M. (2014). Basement membrane and cell integrity of self-tissues in maintaining Drosophila immunological tolerance. *PLoS Genet* **10**, e1004683.

Papagiannouli, F., Schardt, L., Grajcarek, J., Ha, N. and Lohmann, I. (2014). The Hox gene Abd-B controls stem cell niche function in the Drosophila testis. *Dev Cell* **28**, 189-202.

Prasad, M., Jang, A. C., Starz-Gaiano, M., Melani, M. and Montell, D. J. (2007). A protocol for culturing Drosophila melanogaster stage 9 egg chambers for live imaging. *Nat Protoc* **2**, 2467-2473.